frontiers in Physics

BRIEF RESEARCH REPORT
published: 10 March 2022
doi: 10.3389/fphy.2022.820177

Compound Cavity Passively Q-Switched Single-Longitudinal-Mode Diode-Pumped Laser

Bin Chen[1,2], *Zhenxu Bai*[1,2]*, *Guijuan Zhao*[1,2], *Yu Zhang*[1,2], *Bingzheng Yan*[1,2], *Yaoyao Qi*[1,2], *Jie Ding*[1,2], *Kun Wang*[3], *Yulei Wang*[1,2] and *Zhiwei Lu*[1,2]*

[1]Center for Advanced Laser Technology, Hebei University of Technology, Tianjin, China, [2]Hebei Key Laboratory of Advanced Laser Technology and Equipment, Tianjin, China, [3]School of Energy and Environmental Engineering, Hebei University of Technology, Tianjin, China

A compact solid-state single-longitudinal-mode (SLM) Q-switched laser based on a compound cavity is demonstrated. SLM operation is achieved through the enhancement of mode competition (*via* manipulation of the effective reflectivity of the resonator mirrors and intracavity field accumulation time) and does not require the use of a feedback loop. In this work, SLM emission with a linewidth of 254.3 MHz is demonstrated, and a high SLM ratio of up to 99.6% is achieved. The laser operates at a repetition rate of 10 Hz, producing 10 ns pulses with a pulse energy of 14.81 mJ.

Keywords: single-longitudinal-mode, self-seed injection, passively Q-switched, laser technique, compound cavity

OPEN ACCESS

Edited by:
Yufei Ma,
Harbin Institute of Technology, China

Reviewed by:
Zhenqiang Chen,
Jinan University, China
Quan Sheng,
Tianjin University, China

***Correspondence:**
Zhenxu Bai
baizhenxu@hotmail.com
Zhiwei Lu
zhiweilv@hebut.edu.cn

Specialty section:
This article was submitted to Optics and Photonics, a section of the journal Frontiers in Physics

Received: *22 November 2021*
Accepted: *19 January 2022*
Published: *10 March 2022*

Citation:
Chen B, Bai Z, Zhao G, Zhang Y, Yan B, Qi Y, Ding J, Wang K, Wang Y and Lu Z (2022) Compound Cavity Passively Q-Switched Single-Longitudinal-Mode Diode-Pumped Laser. Front. Phys. 10:820177. doi: 10.3389/fphy.2022.820177

INTRODUCTION

In recent years, lasers with different spectral and time-domain characteristics have been widely used in spectral detection, space exploration, manufacturing, etc. [1–4]. Across the domains of coherent optical communications, sodium guide star technology, gravitational wave detection, and non-linear optics, solid-state single-longitudinal-mode (SLM) laser sources with a narrow spectral bandwidth are attracting significant interest [5–10]. These lasers, which often also carry additional characteristics such as broad wavelength tuning capability, high pulse energy, and good beam quality, are enabling a host of new techniques and methodologies. SLM laser sources that operate in the near-infrared spectral region are also gaining traction as the ideal laser sources for molecular spectroscopy [11].

From a practical standpoint, lasers which operate with a SLM must have an effective means of eliminating the spikes created by the beat frequency of adjoining longitudinal modes; this is because these spikes are the most common source of damage to laser system components [12–14]. A number of methods have been used to produce SLM output from solid-state lasers include twisted-mode cavities (TMC) [15], ring cavities [16], the application of etalons or gratings [17–19], microchip lasers [15, 16], and seed injection lasers [20, 21]. However, it should be noted that many of these approaches yield laser outputs with quite low SLM ratio (herein defined as the ratio of the number of single longitudinal mode pulses to the total number of pulses in a certain time). This is due to the wide gain bandwidth and narrow longitudinal mode spacing which is a common characteristic of solid-state lasers. Recent demonstrations (circa 2016–2020) of SLM output from a number of different solid-state laser designs are summarized in **Table 1**. Here the summary focusses on advancements in cavity design and mode-selecting/isolating capability.

The prior literature shows that the primary approaches to generating SLM output are based on threshold regulation and mode competition enhancement [18–24]. In comparison to ring cavities, it

TABLE 1 | Summary of recently reported SLM lasers.

Author(s)	Resonant cavity layout	SLM selection mechanism	Output characteristics
Zhenxu Bai et al. [22], (2016)	Standing wave cavity	Three-plane resonant reflector and saturable absorber	M^2: 1.45 Pulse width: 10.7 ns Pulse energy: 10 mJ (10 Hz) Linewidth: <2.9 GHz
Wencai Li et al. [23], (2017)	Fiber ring cavity	Seed injection	Repetition rate: 1–100 kHz Pulse width: 50–400 ns Pulse energy: 3 μJ (1 kHz) Linewidth: 1.5 MHz
Feng Xue et al. [16], (2018)	Ring cavity	F-P etalon and saturable absorber	M^2: 1.35 Pulse width: 43 ns Pulse energy: 431 μJ Linewidth: <132.5 MHz
ShuTao Dai et al. [24], (2018)	Self-filtering unstable cavity	Seed injection	Pulse width: 16 ns Pulse energy: 50 mJ Energy fluctuation: 1.05% Linewidth: <132.5 MHz
Long Jin et al. [19], (2020)	Standing wave cavity	F-P etalon and Q-switched pre-lasing	Repetition rate: 10 kHz Pulse width: 81.1 ns Pulse energy: 3.94 μJ Linewidth: 33 MHz
I. G. Marienko et al. [25], (2020)	Standing wave cavity	Seed injection and dispersive prism	Slope efficiency: 43% Pulse width: 8 ns Pulse energy: 6 mJ Linewidth: 100 MHz
Duo Jin et al. [15], (2020)	Standing wave cavity	Three-plane resonant reflector, saturable absorber and TMC	SLM ratio: 96.2% Pulse width: 9.8 ns Symmetric pulses: 0.64

is commonly shown that standing wave cavities can generate higher energy pulses with narrower pulse width and with minor beam distortion. A standing-wave cavity is also more desirable from a practical standpoint as it is often more robust and easier to handle in comparison to a ring cavity design. Additionally, standing wave cavities may quite easily integrate with mode selection devices/approaches such as injection-seeding and Fabry-Perrot (F-P) etalons to produce SLM output [19, 25]. It should be noted that the emission from SLM lasers which make use of passive mode selection techniques (TMC and three-plane resonant reflector) typically exhibit inferior SLM ratio unless multiple intracavity components are used [15]. In this case, the insertion of multiple components (such as F-P etalons) increases the loss within the cavity and limits energy output [19, 26]. Injection-seeding can be used to achieve a high SLM ratio; however, it is a bulky, costly, and complicated approach which also typically requires high maintenance. Cavity-stabilization loops are also a source of significant technical complications for injection-seeded lasers [25, 27]. There is, hence, a need for new and novel approaches which may improve the simplicity, robustness, and affordability of high SLM ratio lasers.

One such approach which may address this need is to utilize a mode selection strategy based on a compound cavity combined with a TMC. Here, a compound cavity comprising two distinct cavities is used for longitudinal mode selection, replacing conventional devices such as etalons or gratings. The application of a compound cavity increases mode competition within the laser and also acts as a frequency-selector, suppressing

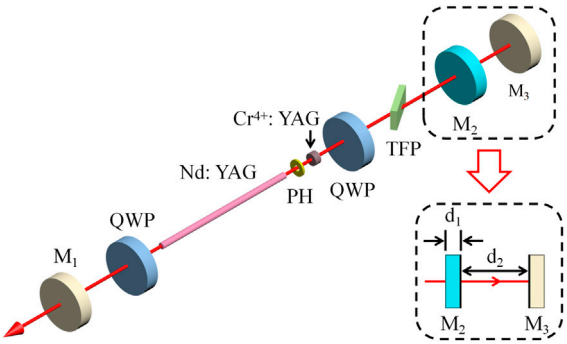

FIGURE 1 | Schematic diagram of the compound cavity passively Q-switched single-longitudinal-mode diode-pumped laser. QWP, quarter-wave plate; PH, pinhole; TFP, thin-film polarizer. (Illustration: resonant mirror frequency selector.)

numerous longitudinal and transverse modes. The above feature is the main difference between the compound cavity and the three-plane resonant reflector. In the three-plane resonant reflector, the inserted mirror is coupled with the output mirror for use as the output mirror. In this work, a compound cavity was integrated into a passively Q-switched, standing wave cavity which provided significant round-trip gain. The long transit time of the laser field within the passively Q-switched cavity was beneficial in limiting the generation of multiple-longitudinal-modes. The considerable laser gain combined with small initial transmittance of the passive Q-switch was conducive to obtaining

laser pulses with a short pulse duration and high peak power. The TMC (formed using quarter wave plates) was integrated into the laser as a means of limiting the effect of spatial hole burning; this further improved the laser's single-mode operation. The laser was capable of operating with output pulse frequencies from 1 to 10 Hz with high energy stability (the root mean square energy fluctuation was <1%).

EXPERIMENTAL SETUP AND NUMERICAL ANALYSIS

The setup of the compound cavity, passively Q-switched SLM diode-pumped laser device is shown in **Figure 1**. The physical length of the cavity was 420 mm. The back cavity mirror M_3 and the resonant mirror M_2 constituted a resonant sub-cavity. Quarter-wave plates (QWPs) were used to form a TMC which limited the spatial hole burning in the laser gain medium. The front cavity mirror M_1 had a reflectivity of 60% at 1,064 nm. The resonant mirror M_2 had a reflectivity of 10% at 1,064 nm on the side facing mirror M_3, and was anti-reflection coated (for 1,064 nm) on the side facing mirror M_1. The back cavity mirror M_3 had a reflectivity of more than 99.5% at 1,064 nm. The laser gain medium was an Nd:YAG (Φ 3 × 78 mm) crystal with a 1% Nd^{3+} doping concentration; both faces of the crystal were coated anti-reflecting at 1,064 nm. A diode pump laser with a repetition rate of 10 Hz and a pulse duration of 250 μs was used in a side-pumping configuration (this was done so as to minimize thermal loading within the laser crystal). The laser was passively Q-switched by a saturable absorber Cr^{4+}:YAG crystal (Φ 6 × 3.25 mm), which had an initial transmittance of 12.23%. The laser produced Q-switched output when the pump energy was ~0.5 J. The laser was p-polarized via the inclusion of a thin-film polarizer (TFP); a 2 mm pinhole (PH) was used to control the intracavity transverse modes.

In **Figure 1**, the resonant mirror (M_2) is used to induce frequency selection within the laser. The means by which this is achieved can be modeled theoretically using thin-film analysis methods in combination with laser signal build-up times. Such an analysis is presented below. We start by calculating the transmission matrix. As outlined in **Figure 1**, for a plate of thickness d_1, and plate separation of d_2, the transmission matrix is given by [28]:

$$M_j = \begin{bmatrix} \cos\delta_j & -\frac{i}{n_j}\sin\delta_j \\ -in_j\sin\delta_j & \cos\delta_j \end{bmatrix} \tag{1}$$

where δ_j is the phase delay of light passing through the medium. The expression of δ_j is given by:

$$\delta_j = \frac{2\pi}{\lambda} n_j d_j \cos\theta_j \tag{2}$$

where n and d are the refractive index and thickness of the jth media, respectively. λ and θ are the incident wavelength and angle of incidence, respectively. The total transmission matrix is expressed as:

$$M = \prod_i M_i = \begin{bmatrix} m_{11} & im_{12} \\ im_{21} & m_{22} \end{bmatrix} \tag{3}$$

The combined reflectivity of the compound frequency selector system as a function of wavelength is then given by:

$$R(\lambda) = \frac{(m_{11}P_0 - m_{22}P_1)^2 + (m_{12}P_1 \cdot P_0 - m_{21})^2}{(m_{11}P_0 + m_{22}P_1)^2 + (m_{12}P_1P_0 + m_{21})^2} \tag{4}$$

where P_0 and P_1 are the parameters which depend on the medium in which both ends of the resonant reflector system are placed. If placed in air, then $P_0 = P_1 = \cos\theta_0$.

In this work, the thickness of the resonant mirror M_2 is d_1 = 6.35 mm, and the refractive index is 1.51. The distance between M_2 and M_3 is d_2 = 5 cm. From this, one can calculate the combined reflectivity of the system, as a function of wavelength. This was done for the wavelength range 1,063.8–1,064.4 nm in 0.01 pm steps, and this is shown as the blue plot in **Figure 2A**. The envelope period of the reflectivity depends on d_1, and the period of the fine structure depends on d_2. When the separation distance is greater than the thickness, such a structure has a peak reflection of 40%. When this occurs, the reflectivity of M_2 is less than M_1, and M_2 becomes the output mirror of the sub-resonant cavity.

When the laser is operating in a low gain state, the round-trip gain is [15]:

$$G = R\left(T_0T_pT_d\right)^2 \exp\left[2g_0l\frac{(\Delta\lambda/2)^2}{(\lambda-\lambda_0)^2 + (\Delta\lambda/2)^2}\right] \tag{5}$$

where T_0, T_p and T_d are the initial transmittance of the Cr^{4+}: YAG, the transmittance of the TFP, and the transmittance of the PH, respectively. Δλ is the fluorescence linewidth of the gain medium, and g_0 is the small-signal gain coefficient at the laser center wavelength. l is the length of the gain medium, and R is the reflectivity of the resonant mirror frequency selector (as detailed above).

In a standing wave cavity, the number of longitudinal modes of oscillation in the resonant cavity is determined by the gain linewidth Δv of the gain medium and the longitudinal mode interval Δv_q of the resonant cavity. The gain linewidth of Nd:YAG is Δv_0 = 200 GHz, and the longitudinal mode interval of the resonant cavity is $\Delta v_q = c/2L$, where c is the speed of light and L is the optical length of the resonant cavity. Note also that in a compound cavity laser design, longitudinal modes of the resonant cavity must also be supported within the compound cavity if they are to oscillate.

The net gain difference between two adjacent longitudinal modes is proportional to the transit time. Therefore, as the transit time increases, the desired signal gradually accumulates from noise, while at the same time suppressing other longitudinal modes [29]. For passively Q-switched lasers, the laser field build-up process typically requires hundreds to thousands of transits, and this is conducive to the accumulation of laser gain and energy

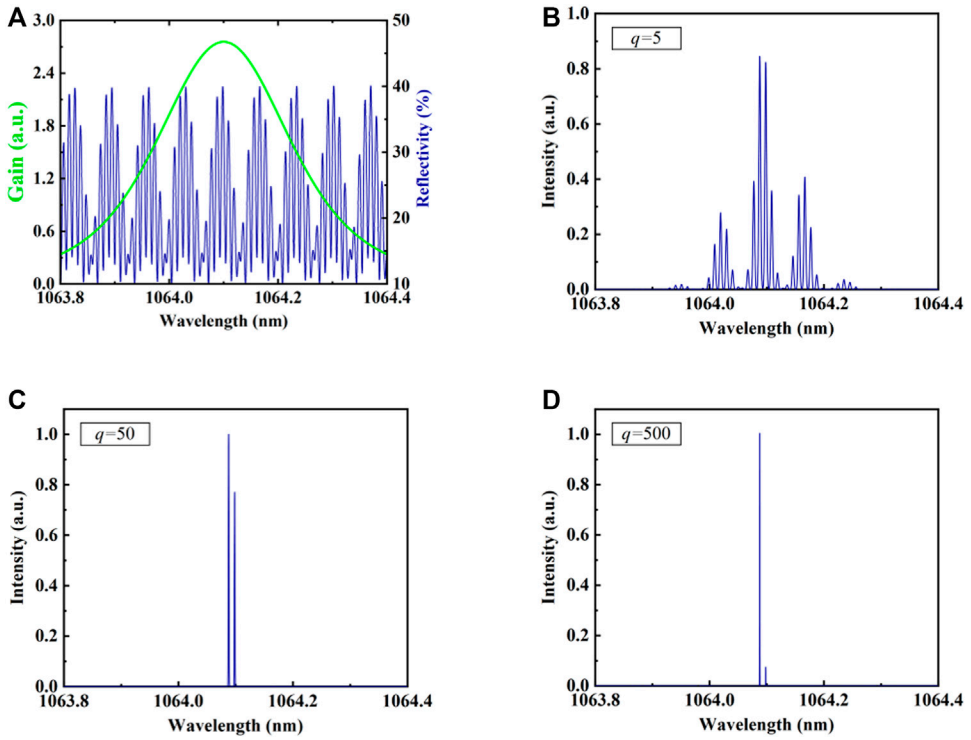

FIGURE 2 | (A) Gain spectrum (green trace) and the reflectivity of the resonant mirror (blue trace) as a function of laser wavelength; **(B)** modeled laser spectrum as a function of wavelength for q = 5 transits; **(C)** modeled laser spectrum as a function of wavelength for q = 50 transits; and **(D)** modeled laser spectrum as a function of wavelength for q = 500 transits.

within a SLM, with a high SLM ratio [30]. The number of loop transits (or round trips) that a laser field undertakes during its build-up from noise to typical output power levels is given by q [28, 31]. It has been calculated that passively Q-switched systems typically require $q > 500$ before the field is output.

In a practical laser, the difference in gain between two adjacent longitudinal modes can be a mere 0.5%. Nevertheless, this minor difference in gain is significant in the context of laser systems wherein laser modes build from noise to megawatt power levels; here the laser modes with the lowest losses emerge as the dominant modes. This effect can be demonstrated through modeling of the laser spectrum. The theoretical spectrum of the laser in this work was modeled for increasing numbers of transits (q) and the resultant spectra are shown in **Figures 2B–D**. It can be seen from the figures that as the number of transits increase, there is a progressive decrease in the number of gain regions that are present in the spectrum. In the case of q = 500 transits, the difference in intensity between the primary gain region and its adjacent neighbor is more than an order of magnitude.

EXPERIMENTAL RESULTS AND DISCUSSION

As this system does not require the use of additional external components (such as piezoelectric transducers and external circuits) to actively adjust cavity mirrors, and does not need injection seeding, the laser system is inherently simple, low cost, and easy to maintain.

The experimental results showed that the insertion angle of the resonant mirror (M_2) had a significant effect on the output characteristics of the laser. When the insertion angle was large (>1°), the insertion of a resonant mirror would lead to significant loss and poor energy stability, resulting in an increase in the laser threshold and linear jitter of the output beam. The spatial characteristics of the output beam were recorded with a laser beam profiler (DataRay WinCamd-LCM). Images of the near-field spatial profiles of the laser output for a range of mirror M_2 insertion angles (<0.1°) are shown in **Figure 3A**. The plots show that a near-perfect Gaussian-like output spot is generated when mirror M_2 is aligned perfectly parallel with the primary laser cavity (formed by mirrors M_1 and M_3). Angular deviation of M_2 led to the formation of two distinct cavities within the laser system. This resulted in undesired oscillation of transverse modes and mode competition. The end result was a reduction in output energy and stability, and deterioration of the mode profile. The system also exhibited some sensitivity to fluctuations in the ambient temperature and the temperature of the water used to cool the laser gain crystal. These fluctuations in the range of ±1°C had the effect of changing the length of the laser cavity and drove mode jumps and occasionally multi-longitudinal mode operation [25]. It is anticipated that this sensitivity can be overcome through simple engineering to improve the temperature-stability of the system.

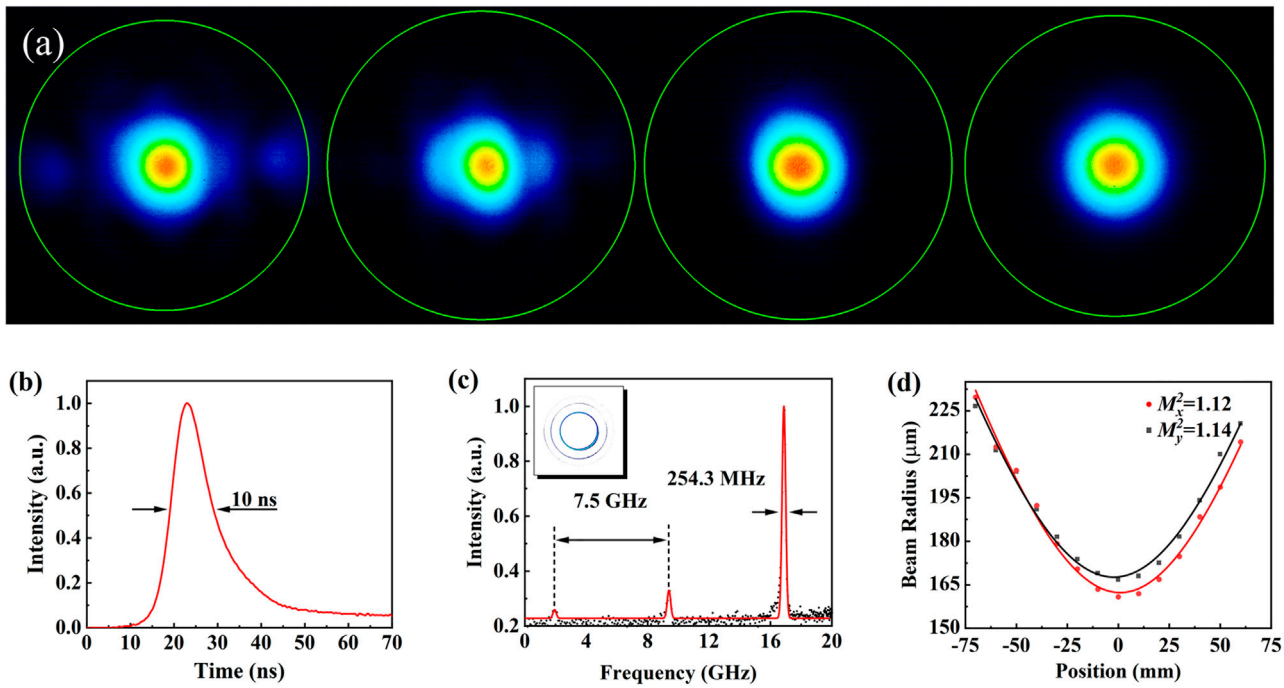

FIGURE 3 | (A) Near-field intensity distribution of the laser output for different M_2 insertion angles from 0.1 to 0° (left-to-right); **(B)** plot of a typical laser output pulse at maximum pulse energy; **(C)** plot of the laser output linewidth as determined using a Fabry-Perot interferometer (inset: typical interferogram from the Fabry-Perot interferometer); and **(D)** plot of the laser beam propagation characteristics and fits used for determination of the beam quality factor.

The output energy was measured using a laser energy meter (OPHIR PE50BB-DIF-C and OPHIR NOVA II). The average pulse energy was 14.81 mJ (at a pump energy of about 0.5 J), and the pulse energy fluctuation was 0.82% over 10,000 shots (taken over a period of ~1 h). The temporal waveform of the output was detected using a fast photodetector (THORLABS DET08C) and was recorded on an oscilloscope (Tektronix MSO64). The pulse shape of the output is shown in **Figure 3B**. The average pulse width was 10.18 ns. Due to the long time required for passive Q-switching to turn off completely when operating at high pump energy, there is a slight tail in the output pulse. It was observed that the TMC had the effect of removing secondary emission peaks in the output when operating at high pump energies.

A home-made Fabry-Perot interferometer with a 7.5 GHz free spectral range and 144 MHz bandwidth was used to examine the spectral properties of the laser output. The emission spectrum of the laser output is shown in **Figure 3C**; also shown inset is an interferogram of the output. The single ring in each interference order indicates that the laser operates with a SLM. The spectrum shows that the laser output linewidth is 254.3 MHz. We believe that this relatively broad linewidth is the result of the length of the laser cavity and the time required for the passive Q-switched to establish oscillation. The SLM ratio of the laser was determined in real-time by examining the output waveform and looking for the presence of any beat frequency components (using the oscilloscope). The measured SLM ratio was ~99.6% over 3,000 shots. Under the same experimental conditions, when TMC is used without a compound cavity, the output waveform is unstable, and it is difficult to achieve SLM ratios greater than 95%.

The beam quality factor of the output was measured, as shown in **Figure 3D**. Standard Gaussian beam propagation fits were used to determine beam quality factors in the *x* and *y* directions of 1.12 and 1.14, respectively. We believe that the significantly better beam quality in this work in comparison to the work summarized in **Table 1** results from the PH and the resonant mirror controlling the transverse modes within the cavity. Future work is focused on reducing the overall cavity length, improving the cavity engineering to achieve stable SLM output without mode hopping, and to investigate methods of further increasing energy output.

CONCLUSION

In conclusion, a pulsed laser utilizing a compound cavity, which operates in SLM with no active cavity stabilization, has been demonstrated. The output has a SLM ratio of 99.6% and a linewidth of 253.4 MHz at a repetition rate of 10 Hz. The pulse width was 10.18 ns, and the average beam quality factor was 1.13. The average pulse energy was 14.81 mJ, with 0.82% pulse energy fluctuations as measured over a 1-h stability test. The compound cavity proposed in this paper has the advantages of a high SLM ratio, high single pulse energy, high energy stability, low cost, compact structure, and is comparatively low maintenance.

DATA AVAILABILITY STATEMENT

The raw data supporting the conclusion of this article will be made available by the authors, without undue reservation.

AUTHOR CONTRIBUTIONS

BC: design of the study, investigation, data curation, writing—original draft. ZB: methodology, writing—review and editing, and supervision. GZ: methodology, data curation, and investigation. YZ: methodology, data curation, and investigation. BY: investigation, writing—original draft, and writing—review and editing. YQ: investigation, and writing—review and editing. JD: investigation, and writing—review and editing. KW: methodology, and supervision. YW: conceptualization, methodology, and supervision. ZL: conceptualization, methodology, supervision, and funding acquisition. All authors contributed to the article and approved the submitted version.

FUNDING

This work was supported by the National Natural Science Foundation of China (No. 61927815).

REFERENCES

1. Williams RJ, Kitzler O, Bai Z, Sarang S, Jasbeer H, McKay A, et al. High Power Diamond Raman Lasers. *IEEE J Select Top Quan Electron.* (2018) 24(5):1–14. doi:10.1109/jstqe.2018.2827658
2. Liu X, Qiao S, Ma Y. Highly Sensitive Methane Detection Based on Light-Induced Thermoelastic Spectroscopy with a 2.33 μm Diode Laser and Adaptive Savitzky-Golay Filtering. *Opt Express* (2022) 30(2):1304–13. doi:10.1364/oe.446294
3. Liu X, Ma Y. Sensitive Carbon Monoxide Detection Based on Light-Induced Thermoelastic Spectroscopy with a Fiber-Coupled Multipass Cell. *Chin Opt Lett* (2022) 20:031201. doi:10.3788/COL202220.031201
4. Bai Z, Yuan H, Liu Z, Xu P, Gao Q, Williams RJ, et al. Stimulated Brillouin Scattering Materials, Experimental Design and Applications: A Review. *Opt Mater* (2018) 75:626–45. doi:10.1016/j.optmat.2017.10.035
5. Qiao S, Ma Y, He Y, Patimisco P, Sampaolo A, Spagnolo V. Ppt Level Carbon Monoxide Detection Based on Light-Induced Thermoelastic Spectroscopy Exploring Custom Quartz Tuning Forks and a Mid-infrared QCL. *Opt Express* (2021) 29(16):25100–8. doi:10.1364/OE.434128
6. Bode N, Meylahn F, Willke B. Sequential High Power Laser Amplifiers for Gravitational Wave Detection. *Opt Express* (2020) 28(20):29469–78. doi:10.1364/oe.401826
7. Bai Z, Zhao Z, Tian M, Jin D, Pang Y, Li S, et al. A Comprehensive Review on the Development and Applications of Narrow-Linewidth Lasers. In: *Microwave and Optical Technology Letters* (2021). Hoboken: Wiley Online Library. p. 1–12. doi:10.1002/mop.33046
8. Huo X, Qi Y, Zhang Y, Chen B, Bai Z, Ding J, et al. Research Development of 589 nm Laser for Sodium Laser Guide Stars. *Opt Lasers Eng* (2020) 134:106207. doi:10.1016/j.optlaseng.2020.106207
9. Guan H, Novack A, Galfsky T, Ma Y, Fathololoumi S, Horth A, et al. Widely-tunable, Narrow-Linewidth III-V/silicon Hybrid External-Cavity Laser for Coherent Communication. *Opt Express* (2018) 26(7):7920–33. doi:10.1364/oe.26.007920
10. Bai Z, Williams RJ, Kitzler O, Sarang S, Spence DJ, Wang Y, et al. Diamond Brillouin Laser in the Visible. *APL Photon* (2020) 5(3):031301. doi:10.1063/1.5134907
11. Kerdoncuff H, Christensen JB, Lassen M. Quantum Frequency Conversion of Vacuum Squeezed Light to Bright Tunable Blue Squeezed Light and Higher-Order Spatial Modes. *Opt Express* (2021) 29(19):29828–40. doi:10.1364/oe.436325
12. Yang X, Kitzler O, Spence DJ, Williams RJ, Bai Z, Sarang S, et al. Single-frequency 620 nm Diamond Laser at High Power, Stabilized via Harmonic Self-Suppression and Spatial-hole-burning-free Gain. *Opt Lett* (2019) 44(4):839–42. doi:10.1364/ol.44.000839
13. Schuhmann K, Kirch K, Nez F, Pohl R, Wichmann G, Antognini A. Spatial Hole Burning in Thin-Disk Lasers and Twisted-Mode Operation. *Appl Opt* (2018) 57(11):2900–8. doi:10.1364/ao.57.002900
14. Ma Y, He Y, Tong Y, Yu X, Tittel FK. Quartz-tuning-fork Enhanced Photothermal Spectroscopy for Ultra-high Sensitive Trace Gas Detection. *Opt Express* (2018) 26(24):32103–10. doi:10.1364/oe.26.032103
15. Jin D, Bai Z, Wang Q, Chen Y, Liu Z, Fan R, et al. Doubly Q-Switched Single Longitudinal Mode Nd:YAG Laser with Electro-Optical Modulator and Cr^{4+}:YAG. *Opt Commun* (2020) 463:125500. doi:10.1016/j.optcom.2020.125500
16. Xue F, Zhang S, Cong Z, Huang Q, Guan C, Wu Q, et al. Diode-end-pumped Single-Longitudinal-Mode Passively Q-Switched Nd:GGG Laser. *Laser Phys Lett* (2018) 15(3):035001. doi:10.1088/1612-202x/aa9b21
17. Rao CS, Kundu S, Ray AK. SLM Operation of a High Repetition Rate BBO Optical Parametric Oscillator Pumped by DPSSL at 355 nm. *Opt Laser Techn* (2021) 138:106878. doi:10.1016/j.optlastec.2020.106878
18. Wang L, Shen Z, Feng X, Li F, Cao Y, Wang X, et al. Tunable Single-Longitudinal-Mode Fiber Laser Based on a Chirped Fiber Bragg Grating. *Opt Laser Techn* (2020) 121:105775. doi:10.1016/j.optlastec.2019.105775
19. Jin L, Dai W, Yu Y, Dong Y, Jin G. Single Longitudinal Mode Q-Switched Operation of Pr:YLF Laser with Pre-lase and Fabry-Perot Etalon Technology. *Opt Laser Techn* (2020) 129:106294. doi:10.1016/j.optlastec.2020.106294
20. Nägele M, Stoppel K, Dekorsy T. Passively Q-Switched 914 nm Microchip Laser for Lidar Systems. *Opt Express* (2021) 29(15):23799–809. doi:10.1364/oe.432340
21. Marianovich A, Spiekermann S, Brendel M, Wessels P, Neumann J, Weyers M, et al. Wedged Nd:YVO_4 Crystal for Wavelength Tuning of Monolithic Passively Q-Switched Picosecond Microchip Lasers. *Opt Express* (2021) 29(13):19790–5. doi:10.1364/oe.430870
22. Bai Z, Wang Y, Lu Z, Chen Y, Li S, Yuan H, et al. A Single -Longitudinal-Mode Nd:Ce:YAG Q-Switched Laser Based on a Three-Plan Resonant Reflector. *J Russ Laser Res* (2016) 37(4):382–8. doi:10.1007/s10946-016-9585-5
23. Li W, Liu H, Zhang J, Yao B, Feng S, Wei L, et al. Mode-hopping-free Single-Longitudinal-Mode Actively Q-Switched Ring Cavity Fiber Laser with an Injection Seeding Technique. *IEEE Photon J.* (2017) 9(1):1–7. doi:10.1109/jphot.2017.2654999
24. Dai S-T, Wu H-C, Shi F, Deng J, Ge Y, Weng W, et al. Development of an Injection-Seeded Single-Frequency Laser by Using the Phase Modulated Technique. *Chin Phys. B* (2018) 27(5):054212. doi:10.1088/1674-1056/27/5/054212
25. Marienko IG, Zhi M, Khizhnyak AI, Sokolov AV. Injection-seeded Single-Longitudinal-Mode Ti:Sapphire Laser with No Active Stabilization. *Opt Express* (2020) 28(17):25444–59. doi:10.1364/oe.401030
26. Lei Y, Mao A, Li Y, Zhang Y, Liu H, Zhang Y. Research on Single Longitudinal Mode Laser Based on F-P Etalon and Q-Switched Delay. *Optik* (2018) 167:1–6. doi:10.1016/j.ijleo.2018.02.018
27. Wang W, Qi H, Song Z, Guo J, Ni J, Wang C, et al. Seed-injected, Actively Q-Switched Fiber Ring Laser Using an AOM of Zero-Order Transmission. *Opt Commun* (2020) 467:125747. doi:10.1016/j.optcom.2020.125747
28. Chebotayev V, Beterov I, Lisitsyn V. Selection and Self-Locking of Modes in He-Ne Lasers with Non-linear Absorption. *IEEE J Quan Electron.* (1968) 4(5):339. doi:10.1109/jqe.1968.1075149

29. Sooy WR. The Natural Selection of Modes in a Passive Q-Switched Laser. *Appl Phys Lett* (1965) 7(2):36–7. doi:10.1063/1.1754286
30. Cole B, Goldberg L, Trussell CW, Hays A, Schilling BW, McIntosh C. Reduction of Timing Jitter in a Q-Switched Nd:YAG Laser by Direct Bleaching of a Cr^{4+}:YAG Saturable Absorber. *Opt Express* (2009) 17(3):1766–71. doi:10.1364/oe.17.001766
31. Thevar TM, Watson J. Longitudinal Mode Selection in a Dye Q-Switched Ruby Laser: a Comparison between Theoretical and Experimental Results. In: *High-Power Lasers: Solid State, Gas, Excimer, and Other Advanced Lasers*, 2889 (1996). Washington: SPIE (International Society for Optical Engineering). p. 60–9.

Conflict of Interest: The authors declare that the research was conducted in the absence of any commercial or financial relationships that could be construed as a potential conflict of interest.